



Biopolymer-based electrolyte membranes from chitosan incorporated with montmorillonite-crosslinked GPTMS for direct methanol fuel cell

Journal:	<i>RSC Advances</i>
Manuscript ID	RA-ART-10-2015-022420.R1
Article Type:	Paper
Date Submitted by the Author:	10-Dec-2015
Complete List of Authors:	<p>Purwanto, Mochammad ; Institut Teknologi Sepuluh Nopember, Department of Chemistry Atmaja, Lukman ; Institut Teknologi Sepuluh Nopember, Department of Chemistry Mohamed, Mohamad Azuwa; Universiti Teknologi Malaysia, Advanced Membrane Technology Research Centre (AMTEC); Universiti Teknologi Malaysia, Faculty of Petroleum & Renewable Energy Engineering Salleh, Muhammad Taufiq; Universiti Teknologi Malaysia, Advanced Membrane Technology Research Centre, AMTEC Jaafar, Juhana; Universiti Teknologi Malaysia, Advanced Membrane Technology Research Centre (AMTEC); Universiti Teknologi Malaysia, Faculty of Petroleum & Renewable Energy Engineering Ismail, Ahmad; Universiti Teknologi Malaysia, Advanced Membrane Technology Research Centre (AMTEC) Santoso, Mardi ; Institut Teknologi Sepuluh Nopember, Department of Chemistry Widiastuti, Nurul ; Institut Teknologi Sepuluh Nopember, Department of Chemistry</p>
Subject area & keyword:	Films/membranes < Materials



Journal Name

ARTICLE

Biopolymer-based electrolyte membranes from chitosan incorporated with montmorillonite-crosslinked GPTMS for direct methanol fuel cell

Received 00th January 20xx,
Accepted 00th January 20xx

DOI: 10.1039/x0xx00000x

www.rsc.org/

Mochammad Purwanto,^{a,b} Lukman Atmaja,^{b*} Mohamad Azuwa Mohamed,^a M.T. Salleh,^a Juhana Jaafar,^{a*} A.F. Ismail,^a Mardi Santoso,^b Nurul Widiastuti^b

A composite membrane was fabricated from biopolymer chitosan and montmorillonite (MMT) filler as an alternative membrane electrolyte for direct methanol fuel cell (DMFC) application. Prior to improve the organic–inorganic interfacial morphology, the pristine MMT was pre-treated using 3-glicidoxy propyltrimethoxysilane (GPTMS) surface modifier to produce the organophilic MMT (O-MMT). The GPTMS modified MMT was mixed with chitosan in acetic acid solution and cast into membranes. SEM images and FTIR analysis showed that the O-MMT was successfully incorporated into chitosan polymer matrix. Water and methanol uptake of the Ch/O-MMT composite membranes decreased with increasing O-MMT loadings, but the ion exchange capacity (IEC) value increased. The Ch/O-MMT with 5 wt.% O-MMT loading exhibited the best methanol permeability and proton conductivity characteristics among other Ch/O-MMT membranes, which were $3.03 \times 10^{-7} \text{ cm}^2 \cdot \text{s}^{-1}$ and $4.66 \text{ mS} \cdot \text{cm}^{-1}$, respectively. All the results obtained from the study can be used to conclude that chitosan membrane with O-MMT filler is a promising high performance PEM candidate for DMFC application.

Introduction

Direct methanol fuel cell (DMFC) is a type of fuel cell that uses methanol as the fuel to generate electricity. This type of fuel cell has several advantages such as ease of fuel distribution and storage, simple system design, high theoretical efficiency, and high theoretical output energy.^{1,2} Despite its attractive benefits, DMFC is still hampered by slow methanol electro-oxidation at the anode side, and methanol crossover from anode to cathode, which become the major problems for DMFC commercialization.³ Perfluorosulfonic acid (PFSA) membrane, under Nafion[®] commercial brand is a type of PEM that has been used extensively.⁴ This is because it has good chemical and mechanical stability, and high proton conductivity. However, Nafion[®] membrane still has shortcomings for DMFC application including relatively expensive price, high methanol crossover, low temperatures based active membrane, and dehydration problem with decreasing proton conductivity at high temperature.^{5,6}

Chitosan is a natural polysaccharide produced from deacetylation of chitin which can be obtained from shrimp shells.⁷ The advantages of biopolymer chitosan include

biodegradable, non-toxic and hydrophilic. Moreover, due to its solubility in dilute acid solution, has enable chitosan to form a gel, thus it is a good material for membranes synthesis. Acetic acid can be used to dilute chitosan polymer to produce chitosan polymer membrane with high rigidity. The presence of hydroxyl groups in the acetic acid facilitates the dissolution of chitosan via hydrogen bonding with the carboxyl group and amine group from the chitosan.^{8,7,9–11}

Chitosan based inorganic hybrid membrane is a promising organic-inorganic hybrids for the development of high performance proton exchange membrane (PEM).⁹ Hassani and co-worker have successfully combined Nafion[®] with chitosan and carbon nanotubes (CNTs).¹² The chitosan-decorated CNT was able to induce a long-range orientation of conduction nano-channels through the interactions with anionic moieties of Nafion[®], and played an effective role in reducing the methanol permeability. Tripathi and co-worker developed a composite membrane by blending chitosan organic polymer with inorganic materials such as silica.¹³ The chitosan organic-inorganic composite membrane was able to suppress the movement of methanol and maintain the presence of water in the membrane.

Recently, the incorporation of layered silicates and in particular montmorillonite (MMT) in chitosan has been extensively studied^{14–17}. The use of MMT as a filler in biopolymer is interesting due to its environmental and economic importance. Nowadays, development on the chitosan based inorganic hybrid membrane using MMT as the inorganic filler is favourable to improve the chitosan membrane performance for DMFC usage.^{18–20} MMT is a type of clay which consists of

^a Advanced Membrane Technology (AMTEC) Research Centre, Universiti Teknologi Malaysia, 81310 UTM Johor Bahru, Johor, Malaysia

^b Department of Chemistry, Institut Teknologi Sepuluh Nopember, ITS Sukolilo, Surabaya 60111, Indonesia

* Correspondence to: Lukman Atmaja (lukman_at@chem.its.ac.id) and Juhana Jaafar (juhana@petroleum.utm.my)

layers of tetrahedral silica and octahedral alumina. This material has parallel layers structure in interrelated form by electrostatic force between layers. The presence of holes in its lattice structure and hydroxyl groups on its surface gives MMT good adsorption characteristics and good compatibility with organic compounds. Furthermore, due to its layered structure, the MMT exhibits large specific surface area, thus gives the MMT good cation exchange capacity and adhesive ability.²¹

High proton conductivity and low methanol permeability of PEM is the key factor to achieve high performance DMFC.²² For organic-inorganic composite membrane, good interaction between the matrix and filler is crucial to develop a membrane with high proton conductivity and low methanol permeability.²¹ MMT as an inorganic material that cannot collaborate perfectly with organic polymer, because the surface layer of montmorillonite cannot interact maximally with the organic portion of the polymer. Organophilization process is one of the promising methods to improve the interaction of MMT in polymer matrices.^{23–25} In 2007, Hong Wu and colleagues successfully improved the interaction of zeolite in chitosan matrices by introducing the 3-Aminopropyltriethoxysilane (APTES) on the surface of the zeolite filler.⁵ Wang et al. (2010) developed Chitosan membranes filled by GPTMS-modified zeolite beta particles with low methanol permeability for DMFC.²⁶ Their study indicated that by using (3-glycidoxypopyl) trimethoxysilane (GPTMS) to modify the zeolite surface, the new developed composite membrane was able to achieve denser and stronger surface morphology. GPTMS is a crosslinking agent that has two functional groups, one is an organic functional group which can form bonding with organic materials, and the other one is an epoxy group which can interact with inorganic materials.²⁷ However, to the best of our knowledge, there is yet any research attempt on immobilized modified MMT using GPTMS in chitosan biopolymer matrices for DMFC application. Therefore, it is crucial to study the feasibility of GPTMS-MMT as filler in chitosan biopolymer matrices with enhanced dispersibility and physicochemicals characteristics for DMFCs.

The aim of this study is to develop a low cost and environmental friendly chitosan/GPTMS-MMT composite membrane from shrimp waste with a high selectivity towards proton conductivity against methanol permeability for DMFC applications. The composite membrane morphology and interactions analysis are conducted using SEM and FTIR. The physicochemical characterizations by means of water uptake, ion exchange capacity, proton conductivity, and methanol permeability are carried out to determine the overall membrane performance for DMFC applications.

Experimental

Materials

Dried shrimp shell powder of *penaeus monodon* was used the chitosan source. Montmorillonite (MMT) powder, 3-glycidoxypopyltrimethoxysilane (GPTMS), and phosphotungstic acid (PTA) were purchased from Sigma-Aldrich. Sodium hydroxide

(NaOH), hydrochloric acid (HCl), methanol (MeOH), acetic acid, hydrogen peroxide (H₂O₂), sulfuric acid (H₂SO₄), toluene, ethanol (EtOH), phenolphthalein indicator, and sodium chloride in pure analytical grade were purchased from Merck.

MMT surface modification

2 g of MMT, 4 g GPTMS, and 40 g of toluene were mixed in a reactor. The reaction was carried out at toluene refluxing temperature (110°C) and stirred for 24 hours. Then, the mixture was filtered and the resulting precipitate was washed with EtOH three times before being soaked in 0.1 M HCl solution for 24 hours at room temperature. The precipitate was then filtered and washed with demineralized water until neutral pH was achieved. Finally, the precipitate was dried in the oven at 100°C for 4 hours. The resulting dry powder was denoted as G-MMT.

Extraction of chitosan

Chitosan was extracted from dried shrimp shell powder of *penaeus monodon* according to a previous study.²⁸ Briefly, the dried shrimp powder was added into 3.5 % NaOH solution with a ratio of 1:10 (w/v) under continuous stirring for 2 hours at 65 °C. Then, the mixture was filtered and resulting was washed until pH 7 and dried at 105 °C. The dried powder was then demineralized using 1 M HCl, stirred for 30 minutes at 65 °C with a ratio of 1:15 (w/v), washed, and dried. The chitin powder obtained was then run through the deacetylation process using 50 % NaOH solution, stirred for four hours at 120 °C with a ratio of 1:10 (w/v), washed, and dried until it became dried powder called chitosan.

Membrane fabrication

Chitosan powder was dissolved in 25 mL of 2 % acetic acid, and stirred at 80 °C and 400 rpm. Another 25 mL of 2 % acetic acid was used to dilute the G-MMT powder and sonicated for 30 minutes. Then, both mixtures were mixed together and stirred for 30 minutes at 80°C. After that, the mixture was given an ultrasonic treatment for 30 minutes, stopped for 30 minutes, and then sonicated again for 30 minutes. After degasification, the mixture was then cast on a glass panel and dried at room temperature for 48 hours.¹¹ The detached membrane was then immersed in 1 M NaOH for 15 minutes before being washed with distilled water until neutral pH was achieved. The membrane then underwent crosslinking process by immersing the membrane in 2 % w/v of phosphotungstic acid (PTA) solution for 24 hours, and then washed repeatedly with distilled water to remove the remaining PTA acid before being dried at room temperature for 24 hours [18]. The compositions of Ch/G-MMT membranes are tabulated in Table 1.

Table 1. Compositions of Ch/G-MMT composite membranes

Membrane characterization

Fourier transform infrared spectroscopy (FTIR) was used to analyse the structure and functional group. The disk containing 0.1–0.2 g sample and 0.5–1.0 g of fine grade KBr was mixed and crushed into powder, and pellets were formed with a hydraulic press. All measurements were scanned within the wave range of 650–4000 cm^{-1} . The morphological structural of the resultant material was analyzed by scanning electron microscopy (SEM) and EDX Bruker analysis. Thermal stability of the samples was characterized using thermogravimetric analysis (TGA). Dry sample was ground into fine powder and the sample was placed in a platinum pan. The analysis was carried out at a heating rate of 10 $^{\circ}\text{C}/\text{min}$ over 30 – 730 $^{\circ}\text{C}$ temperature range under air atmosphere. The sample powder was prepared in the pin stub holder and coated with gold for analysis. Water and methanol uptake were calculated using equation (1).¹¹

$$\text{Uptake}(\%) = \frac{W_{\text{wet}} - W_{\text{dry}}}{W_{\text{dry}}} \times 100\% \quad (1)$$

where W_{dry} and W_{wet} are the membrane weight before and after immersion in gram, respectively. The membrane was dried at 50 $^{\circ}\text{C}$ for 24 h and weighed. Then, the membrane was immersed in water or methanol for 24 h until the membrane was fully hydrated. Then the membrane was removed and gently rubbed with a tissue before being weighed to remove the excess water/methanol on its surface. The ion exchange capacity (IEC) value was determined using titration technique. The membrane was dried at 50 $^{\circ}\text{C}$ for 24 hours, and weighed. Then the membrane was soaked in 50 mL of 1 M NaCl solution to exchange the H^{+} ions in the membrane matrix with Na^{+} . The solution was titrated with 0.01 M NaOH. 1 wt. % phenolphthalein in ethanol solution was used as an indicator. IEC was calculated using equation (2);²⁹

$$\text{IEC} (\text{mmol.g}^{-1}) = \frac{M_{\text{NaOH}} \times 1000 \times V_{\text{NaOH}}}{W_{\text{dry}}} \quad (2)$$

where M_{NaOH} (mol.L^{-1}) and V_{NaOH} (L) are the concentration and volume of NaOH used for titration, and W_{dry} is the membrane's dry weight (g). Methanol permeability was determined using a two-compartment diffusion cell. Compartment A was filled with 1 M MeOH solution and compartment B was filled with deionized water. The membrane was placed between compartment A and B. Samples from compartment B were taken out every 30 minutes for 6 hours to determine its methanol concentration using high-performance liquid chromatography (HPLC). The methanol permeability values were determined by using equation (3).¹⁸

$$P = \left(\frac{\Delta C_B}{\Delta t} \right) \left(\frac{L V_B}{A C_A} \right) \quad (3)$$

P is methanol permeability of the membrane ($\text{cm}^2 \cdot \text{s}^{-1}$), $\Delta C_B / \Delta t$ is the slope variation of methanol concentration in compartment B as a function of time ($\text{mol.L}^{-1} \cdot \text{s}^{-1}$), L is the thickness of the membrane (cm), V_B is the volume of the water at compartment A (cm^3), A is the membrane surface area

(cm^2), and C_A is the concentration of methanol in the cell A (mol.L^{-1}). The proton conductivity of the membrane was measured using electrochemical impedance spectroscopy (EIS), at a frequency of 1–10⁶ Hz. The proton conductivity values were calculated using equation (4);¹⁸

$$\sigma = \frac{L}{R \times A} \quad (4)$$

where σ is the proton conductivity of the membrane (S cm^{-1}), L is the membrane (cm), A is the membrane surface area (cm^2), and R is the membrane resistance (Ω).

Results and discussion

Characterization of G-MMT

Figure 1 shows the SEM images of MMT and G-MMT particles. It appears that before the modification process, the MMT particles visible surfaces were smooth and flat as shown in Figure 1 (a). After being modified with GPTMS (see Figure 1 (b)), the G-MMT particles were rough and overgrown soft granules were spread almost evenly throughout its surface. The incorporation of GPTMS on MMT surface was able to increase oxygen, silica, and alumina compound intensity, as shown in the EDX spectra of G-MMT. These three elements are crucial for bonding formation with chitosan organic polymer, enhancing the mechanical strength of its composite membrane, and developing the trajectory tracks for protons, thus consequently improve the membrane proton conductivity.

Fig. 1 SEM images of (a) MMT, (b) O-MMT and (c) its EDX spectra.

The surface chemistry analysis of MMT before and after its surface modification were investigated by FTIR analysis. As shown in Figure 2, the two peaks at 3440 and 1640 cm^{-1} corresponded to the –OH stretching and bending vibrations of H–O–H on the MMT surface, respectively.¹¹ The GPTMS modification performed on MMT was able to reduce the intensity of –OH stretching bond vibration of pure MMT. This phenomenon describes the consumption of the MMT hydroxyl groups by condensing with the silanol groups.⁵ The MMT surface modification also decreased the water adsorption on its surface due to the bonding formation between MMT and GPTMS.¹¹ The FTIR spectra corresponding to the characteristic peaks of MMT structure which was assigned to Si–O and Al–O stretched at 2880–2940 cm^{-1} and 1000–1300 cm^{-1} , respectively, indicating that the main structure of MMT still exists after the surface modification by GPTMS.³⁰ The FTIR results suggested that the GPTMS has been successfully incorporated into the MMT surfaces, in accordance to SEM and EDX characterization.

Fig. 2. FTIR spectra of (a) MMT and (b) O-MMT.

Chemical interaction and morphological characteristics of Ch/G-MMT composite membrane

FTIR spectra for pure chitosan membrane and Ch/G-MMT composite membrane are presented in Figure 3 (a). It can be seen that the characteristic bands of pure chitosan membrane were recorded at 3350 cm^{-1} , 1650 cm^{-1} , and 1560 cm^{-1} which were attributed to hydroxyl group, amide I, and amide II groups, respectively.²⁶ The peaks at 2930 , 1390 , and 1030 cm^{-1} were assigned to $-\text{CH}_2$ stretching, $-\text{CH}_2$ bending and C–O stretching, respectively.¹¹ Compared to pure chitosan membrane, the intensity of the hydroxyl group, amide I, and amide II bands in the Ch/G-MMT composite membranes decreased. This phenomenon may be caused by the hydrogen bonds or ionic interaction between the $-\text{OH}$ groups on the surface of the G-MMT and $-\text{OH}$ or $-\text{NH}_2$ groups of the chitosan as shown in Figure 3 (b). Two respective bands at 1030 cm^{-1} and 1010 cm^{-1} of the pure chitosan membrane were merged and shifted to 1040 cm^{-1} due to the overlapping of Si–O bond with the C–O stretching bond.⁵

Fig. 3 (a) FTIR spectra of chitosan membrane and its Ch/O-MMT-10 composite membrane, (b) Schematic illustration of the interaction between hydroxyl groups of O-MMT and hydroxyl groups or amide groups of the chitosan polymer chain.

The morphology analysis for chitosan membrane and its composite are presented in Figure 4. The chitosan membrane showed smooth dense structure, meanwhile the SEM images for Ch/G-MMT-5 and Ch/G-MMT-10 showed a good dispersion of G-MMT filler in the composite membranes. Meanwhile, severe agglomeration of unmodified MMT on the surface of Ch/MMT-5 was observed as shown in Figure 4(b). The presence of hydroxyl group of G-MMT has improved the phase interaction between chitosan and G-MMT due to the interaction between hydroxyl groups of G-MMT and hydroxyl groups or amide groups of the chitosan polymer chain as shown in Figure 3 (b).³¹ The modification using GPTMS was able to improve the dispersibility of G-MMT with chitosan organic polymer, thus produced smooth and homogeneous membrane surface with no or little agglomeration and no pinholes. The absence of pinholes is favourable for the suppression of methanol crossover, thus improves the methanol permeability characteristics of the parent polymer-based membrane.¹¹ However, the Ch/G-MMT membrane with G-MMT loading beyond 10 wt. % showed visible agglomeration of G-MMT on the membrane surface. The agglomeration phenomena occurrence is most probably due to the excessive loading of G-MMT filler which is not completely dissolved during the membranes solution preparation.

Fig. 4: SEM images of (a) pure chitosan, (b) Ch/MMT-5, (c) Ch/G-MMT-5 and (d) Ch/G-MMT-10.

Thermal stability analysis

In this study, TGA/DTG analysis was carried out in an effort to investigate the thermal stability properties of Ch and Ch/G-

MMT. The TGA and DTG curves in Figure 5 show that all samples followed almost identical degradation mechanism since there were miniscule difference in $T_{10\%}$, $T_{30\%}$, $T_{50\%}$, and T_{max} , as shown in Table 2. As shown in the Figure 5, all membranes show three stages of weight loss, the first stage that happens below $175\text{ }^\circ\text{C}$ which was attributed to the lost components such as physically absorbed water.^{32,33} The second weight loss stage occurs at $175\text{--}400\text{ }^\circ\text{C}$, was due to the cleavage of Ch chains and the removal of bound water molecules from PTA. In the third stage, above $400\text{ }^\circ\text{C}$, the weight loss was due to the structure collapse of PTA and the thermal decomposition of glucosamine residues present in Ch.³⁴ It has been reported that the decomposition of montmorillonite clay is not complete until $800\text{ }^\circ\text{C}$.³² Therefore, it is believed that the incorporation of G-MMT inorganic filler into chitosan polymer matrix was able to increase the thermal stability of the new chitosan composite membrane as shown in Figure 5. As can be seen in Table 2, the neat Ch exhibited the lowest in residual percent as compared to Ch/G-MMT composite membrane. The incorporation of GPTMS has improved the interaction of MMT with chitosan by introducing more functional groups (Figure 3 (a)) which allowed the formation of more hydrogen bonding with chitosan polymer chain. Therefore, higher number hydrogen bond formation can be expected in Ch/G-MMT membrane rather than in pure Ch membrane. Consequently, the Ch/G-MMT membrane can be expected to possess higher thermal stability characteristics compared to pure Ch membrane. Therefore, the resultant composite membrane is stable at desired operating temperatures ($<100\text{ }^\circ\text{C}$) for DMFCs application.^{34,33}

Table 2. Thermal Stability data of Ch and Ch/G-MMT 5, 10, and 15%

Fig. 5. TGA and DTG curves of pure chitosan (Ch) and Ch/G-MMT membrane with different G-MMT loading.

Water and methanol uptake

It is crucial for PEM membrane to be able to hold water because the proton will be transported along the water channel created in the membrane polymer matrix. Thus, high water uptake is favourable for high performance PEM to facilitate great numbers of protons hopping and diffusion through the membrane. The water uptake for Ch/G-MMT membranes is shown in Figure 6. The water uptake value for pure chitosan membrane was 72.9%, but as the loading of G-MMT increased, the water uptake decreased. The lowest value of water uptake was recorded by Ch/G-MMT-25 membrane which was 38.1%. Similar observation can also be found elsewhere.³⁵ In addition, Gosawit and co-worker reported in a previous study where the water uptake for SPEEK composite membrane decreased as the sulfonated MMT (S-MMT) loading increased.³⁶ The previous study suggested that the reduction of water uptake occurs because of two reasons; 1) agglomeration of modified MMT and 2) intercalation in clay

layers which might obstruct the polymer chain movement, hence resulted in chain packing. Besides water uptake characteristics, methanol uptake is also one of the important properties to determine the quality of PEM, especially for DMFC applications. High methanol uptake will increase the fuel loss, thus will reduce the fuel efficiency of DMFC. Therefore, it is highly desirable for the PEM to have a small absorption of methanol. Chitosan membrane showed lower methanol uptake than water uptake (67.4% compared to 72.9% at the same G-MMT loading), and increasing the loading of G-MMT will further reduce the methanol uptake of Ch/G-MMT composite membrane. It has been suggested that, this phenomenon is might due to the existence of modified MMT filler which increases the tightness of composite membrane so it can suppress little methanol and diffuses into the membrane composite.³⁷ The modified MMT (G-MMT) can improve the interaction with chitosan matrix via hydrogen bonds. Given the strong interaction, the membrane has a structure that is more dense, thus reducing the movement of methanol into the membrane. Similar observation also can be found elsewhere.³⁸

improve the methanol permeability of the membrane. This is due to the MMT structure that has a high width to length ratio which creates longer diffusion path for methanol to permeate.⁴⁰ However, excessive G-MMT loading will cause agglomeration, thus hampers the G-MMT advantages to reduce methanol permeation rate. From the study, Ch/G-MMT-5 showed the appropriate loading to achieve the lowest methanol permeability value, which is $3.03 \times 10^{-7} \text{ cm}^2 \cdot \text{s}^{-1}$. This result is in agreement with the SEM images, where Ch/G-MMT-5 showed the least G-MMT agglomeration as compared to other loadings.

Table 3. Methanol permeability, proton conductivity, and relative selectivity of pure chitosan and Ch/G-MMT composite membranes.

^atwo probe method, analysis using Autolab instrument

^bcell diffusion method, analysis by HPLC

^cthe chitosan that has been synthesis in this study

Fig. 6. Water and methanol uptake of Ch/G-MMT membranes.

Ion exchange capacity (IEC)

Figure 7 presents the ion exchange capacity (IEC) results for chitosan and Ch/G-MMT composite membranes. The IEC value dropped when 5% of G-MMT was added to the polymer membrane, but higher loading of G-MMT filler increased the IEC value of Ch/G-MMT composite membrane. These results are comparable to the IEC results for SPEEK/MMT-AMPS composite membrane.³⁹ This is due to the presence of G-MMT that has formed good interaction with chitosan which then provides the environment favourable for ion exchange phenomenon in the membrane. One of the desired properties of electrolyte membrane is the ability to exchange ions for the proton mobile platform in the membrane matrices. The highest IEC value found was 2.71 mmol g^{-1} which was recorded by Ch/G-MMT 25 membrane.

Fig. 7 IEC values of Ch/O-MMT membranes with different O-MMT loading (%).

Methanol permeability, proton conductivity, and membrane selectivity.

The methanol permeability, proton conductivity, and membrane selectivity are portrayed in Figure 8. Low methanol permeability is important for PEM in DMFC applications. Since DMFC uses methanol as fuel, low methanol permeability PEM would contribute to high-efficiency fuel usage and low fuel loss. The methanol permeability of pure chitosan and Ch/G-MMT composite membranes is shown in Table 3. Pure chitosan membrane showed good methanol permeability ($4.97 \times 10^{-7} \text{ cm}^3/\text{s}$), which is lower compared to commercial Nafion[®] membrane ($25.00 \times 10^{-7} \text{ cm}^2 \cdot \text{s}^{-1}$). It is suggested that the incorporation of G-MMT to Ch/G-MMT membrane is able to

Proton conductivity is one of the most important properties for proton-conducting membranes used in fuel cell. In general, the proton transport in hydrated polymeric matrices is described on the basis of either two principal mechanisms: "proton hopping" or "Grotthuss mechanism" and "diffusion mechanism" which water as a vehicle or "vehicular mechanism".⁴¹ The proton conductivity for chitosan and Ch/G-MMT composite membranes are listed in Table 3, and compared with the references for Nafion117 and commercial chitosan. In this study, the addition of 5% G-MMT was able to achieve a maximum proton conductivity of $4.66 \text{ mS} \cdot \text{cm}^{-1}$, an increase from $2.36 \text{ mS} \cdot \text{cm}^{-1}$ exhibited by the parent chitosan membrane. The abundance of -OH group on G-MMT surface is able to provide additional conduction site for proton to be transported, thus increases the proton conductivity of the membrane.⁵ In addition, the increment in proton conductivity might be due to the fact that PTA can improve the interaction between Ch and G-MMT at desirable composition. PTA consists of central PO_4 tetrahedron units surrounded by tungsten (W_3O_{13}) units and linked through oxygen atoms. The terminal and anionic oxygen species in PTA are the most reactive among the four oxygen species and can interact with groups in Ch and G-MMT in the composite network structure.⁴² PTA, Ch and G-MMT construct a continuous hydrophilic channels, which allows the protons to be transported via vehicle mechanism in the form of hydronium ions.⁴² It has been suggested that, due to electrostatic interaction between PTA, Ch and G-MMT, Ch/G-MMT membranes which contain the numerous hydroxy group, $-\text{NH}_3^+$ and heteropolyanions, the proton transferred along the ionic bonds and hydrogen bonds by "jumping" from one functional group to another.³³ Therefore, this study suggest that both vehicular mechanism and Grotthuss mechanism are responsible for the proton conductivity of the Ch/G-MMT membranes. However, higher filler loading has led to

agglomerations problem in Ch/G-MMT membrane, hence reduces the effectiveness of G-MMT to provide conduction site for proton. In addition, as seen in Table 3, higher G-MMT loading led to the reduction in membrane water uptake, contributing to the decrease of proton conductivity of the membrane.¹⁸ Low water condition in the membrane composite caused loading structure and the presence of G-MMT that has formed good interaction with chitosan has the ability of exchanging ions for the proton mobile platform in the membrane, so the value of IEC increases while the water uptake and proton conductivity decrease.

Membrane selectivity was used to further assess the performance of Ch/G-MMT composite membrane. For DMFC application, the membrane selectivity is defined as the ratio of proton conductivity to methanol permeability of the membrane. In order to be an excellent PEM membrane for DMFC, high proton conductivity and low methanol permeability PEM are desired. The membrane selectivity reflects the overall membrane characteristics and can be used as an overall performance evaluation factor.⁴⁰ Based on the selectivity value in Table 3, the addition of G-MMT filler is able to promote the performance of chitosan membrane in general. The G-MMT filler is able to provide an additional conductive site for proton transportation, and at the same time it creates longer diffusion path for methanol to permeate, thus improves the membrane methanol permeability. However, excessive G-MMT will reduce the membrane performance because of the G-MMT agglomeration problem, and thus restricts the membrane ability to absorb water. Thus, it is crucial to determine the optimum loading of G-MMT to maximize the Ch/G-MMT potential as PEM for DMFC operation. From Table 2, it can be seen that 5% of G-MMT loading was the best loading to improve the chitosan membrane performance. The Ch/G-MMT 5 exhibited the best proton conductivity and methanol permeability characteristics among other Ch/G-MMT composite membranes.

Fig. 8. Methanol permeability, proton conductivity, and relative selectivity of pure chitosan and Ch/G-MMT composite membranes with different O-MMT loading (%).

Conclusions

Composite biopolymer membrane of chitosan and GPTMS modified MMT was successfully prepared using solution casting method. The presence of more hydroxyl group of G-MMT improved the phase interaction between chitosan and G-MMT due to the interaction between hydroxyl groups of G-MMT and hydroxyl groups or amide groups of the chitosan polymer chain. It has been proven that, the incorporation of G-MMT within chitosan membrane significantly improved the physicochemical properties of the resultants Ch/G-MMT composite membrane. SEM images of Ch/G-MMT-5 and Ch/G-MMT-10 has showed smooth membrane surfaces as the evidence of homogeneously incorporated G-MMT into the chitosan polymer matrix due to superior compatibility

promoted by GPTMS on the surface of MMT. In addition, the thermal stability of Ch/G-MMT composite was improved as compared by pristine chitosan membrane. The water uptake for Ch/G-MMT membranes reduced as the loading of G-MMT increased. The Ch/G-MMT-5 membrane showed the best methanol permeability and proton conductivity values among the Ch/G-MMT composite membranes, thus concludes that 5 wt. % loading of G-MMT filler is the best loading to improve the parent chitosan membrane characteristics. Furthermore, it is trustworthy to note that the incorporation of modified MMT (G-MMT) within the chitosan matrix has significantly surpassed Nafion in term of the methanol permeability and selectivity properties. Based on the obtained results, it can be concluded that chitosan membrane consisting G-MMT filler prepared from shrimp waste has a high potential to be a promising low cost and environmental friendly polymer electrolyte membrane for DMFC applications.

Acknowledgements

The author (Mochammad Purwanto) would like to express gratitude to the Ministry of Science, Technology and Innovation (MOSTI) Malaysia and Ministry of Higher Education for the financial support from the grants with the vote number of R.J130000.7942.4S507, R.J130000.7809.4F592 and Q.J130000.2509.05H52, and also to the research management centre (RMC), Universiti Teknologi Malaysia for supporting the research management activities.

Notes and references

1. A. O. Odeh, P. Osifo, and H. Noemagus, *Energy Sources, Part A Recover. Util. Environ. Eff.*, 2013, **35**, 152–163.
2. C. Spiegel, *Design and Building Fuel Cells*, McGraw-Hill, New York, 2007.
3. Y. S. Kang, N. Jung, K.-H. Choi, M. J. Lee, M. Ahn, Y.-H. Cho, and Y.-E. Sung, *Appl. Surf. Sci.*, 2014, **290**, 246–251.
4. J. L. Lu, Q. H. Fang, S. L. Li, and S. P. Jiang, *J. Memb. Sci.*, 2013, **427**, 101–107.
5. H. Wu, B. Zheng, X. Zheng, J. Wang, W. Yuan, and Z. Jiang, *J. Power Sources*, 2007, **173**, 842–852.
6. F. Lufrano, V. Baglio, P. Staiti, V. Antonucci, and A. S. Arico', *J. Power Sources*, 2013, **243**, 519–534.
7. F. Croisier and C. Jérôme, *Eur. Polym. J.*, 2013, **49**, 780–792.
8. J. Wang and L. Wang, *Solid State Ionics*, 2014, **255**, 96–103.
9. B. P. Tripathi and V. K. Shahi, *Prog. Polym. Sci.*, 2011, **36**, 945–979.
10. C. Chen, Z. Gao, X. Qiu, and S. Hu, *Molecules*, 2013, **18**, 7239–7252.
11. Y. Wang, D. Yang, X. Zheng, Z. Jiang, and J. Li, *J. Power Sources*, 2008, **183**, 454–463.
12. M. M. Hasani-Sadrabadi, E. Dashtimoghdam, F. S. Majedi, S. Wu, A. Bertsch, H. Moaddel, and P. Renaud, *RSC Adv.*, 2013, **3**, 7337.
13. B. P. Tripathi, M. Kumar, A. Saxena, and V. K. Shahi, *J. Colloid Interface Sci.*, 2010, **346**, 54–60.

14. K. Grigoriadi, A. Giannakas, A. K. Ladavos, and N.-M. Barkoula, *Polym. Bull.*, 2015, **72**, 1145–1161.
15. Y. Huang, J. Huang, J. Cai, W. Lin, Q. Lin, F. Wu, and J. Luo, *Carbohydr. Polym.*, 2015, **134**, 390–397.
16. S. I. Hong, J. H. Lee, H. J. Bae, S. Y. Koo, H. S. Lee, J. H. Choi, D. H. Kim, S.-H. Park, and H. J. Park, *J. Appl. Polym. Sci.*, 2011, **119**, 2742–2749.
17. H. Oguzlu and F. Tihminlioglu, *Macromol. Symp.*, 2010, **298**, 91–98.
18. M. Tohidian, S. R. Ghaffarian, S. E. Shakeri, E. Dashtimoghadam, and M. M. Hasani-Sadrabadi, *J. Solid State Electrochem.*, 2013, **17**, 2123–2137.
19. S. E. Shakeri, S. R. Ghaffarian, M. Tohidian, G. Bahlakeh, and S. Taranejoo, *J. Macromol. Sci. Part B*, 2013, **52**, 1226–1241.
20. M. M. Hasani-Sadrabadi, E. Dashtimoghadam, F. S. Majedi, K. Kabiri, N. Mokarram, M. Solati-Hashjin, and H. Moaddel, *Chem. Commun. (Camb.)*, 2010, **46**, 6500–2.
21. M. A. Khedr, A. I. Waly, A. I. Hafez, and H. Ali, *Aust. J. Basic Appl. Sci.*, 2012, **6**, 216–226.
22. J. Jaafar, A. F. Ismail, T. Matsuura, and K. Nagai, *J. Memb. Sci.*, 2011, **382**, 202–211.
23. E. Amendola, *Open Macromol. J.*, 2012, **6**, 33–36.
24. M. Huskić, I. Brnardić, M. Žigon, and M. Ivanković, *J. Non. Cryst. Solids*, 2008, **354**, 3326–3331.
25. N. Jiratumnukul, P. Manowanna, and N. Premmag, *Eng. J.*, 2012, **16**, 13–18.
26. Y. Wang, Z. Jiang, H. Li, and D. Yang, *Chem. Eng. Process. Process Intensif.*, 2010, **49**, 278–285.
27. C.-C. Yang, S. J. Lue, and J.-Y. Shih, *J. Power Sources*, 2011, **196**, 4458–4467.
28. E. Trisnawati, D. Andesti, and A. Saleh, *J. Tek. Kim.*, 2013, **19**, 17–26.
29. T. Xu, W. Hou, X. Shen, H. Wu, X. Li, J. Wang, and Z. Jiang, *J. Power Sources*, 2011, **196**, 4934–4942.
30. R. Jana and H. Bhunia, *Solid State Ionics*, 2008, **178**, 1872–1878.
31. M. A. Mohamed, W. N. W. Salleh, J. Jaafar, A. F. Ismail, M. Abd Mutalib, and S. M. Jamil, *Carbohydr. Polym.*, 2015, **133**, 429–437.
32. B. R. dos Santos, F. B. Bacalhau, T. dos S. Pereira, C. F. Souza, and R. Faez, *Carbohydr. Polym.*, 2015, **127**, 340–6.
33. Z. Cui, W. Xing, C. Liu, J. Liao, and H. Zhang, *J. Power Sources*, 2009, **188**, 24–29.
34. Y. Xiao, Y. Xiang, R. Xiu, and S. Lu, *Carbohydr. Polym.*, 2013, **98**, 233–40.
35. S. E. Shakeri, S. R. Ghaffarian, M. Tohidian, G. Bahlakeh, and S. Taranejoo, *J. Macromol. Sci. Part B*, 2013, **52**, 1226–1241.
36. R. Gosalawit, S. Chirachanchai, S. Shishatskiy, and S. P. Nunes, *J. Memb. Sci.*, 2008, **323**, 337–346.
37. N. K. Shrivastava, S. B. Thombre, and R. B. Chadge, *Ionics (Kiel)*, 2015.
38. P. Bahavan Palani, R. Kannan, S. Rajashabala, S. Rajendran, and G. Velraj, *Ionics (Kiel)*, 2014, **21**, 507–513.
39. M. F. Samberan, M. M. Hasani-Sadrabadi, S. R. Ghaffarian, and A. Alimadadi, *Int. J. Hydrogen Energy*, 2013, **38**, 14076–14084.
40. H. Lin, C. Zhao, W. Ma, K. Shao, H. Li, Y. Zhang, and H. Na, *J. Power Sources*, 2010, **195**, 762–768.
41. S. J. Peighambaroust, S. Rowshanzamir, and M. Amjadi, *Int. J. Hydrogen Energy*, 2010, **35**, 9349–9384.
42. S.-H. Lee, S.-H. Choi, S.-A. Gopalan, K.-P. Lee, and G. Anantha-Iyengar, *Int. J. Hydrogen Energy*, 2014, **39**, 17162–17177.

List Figures

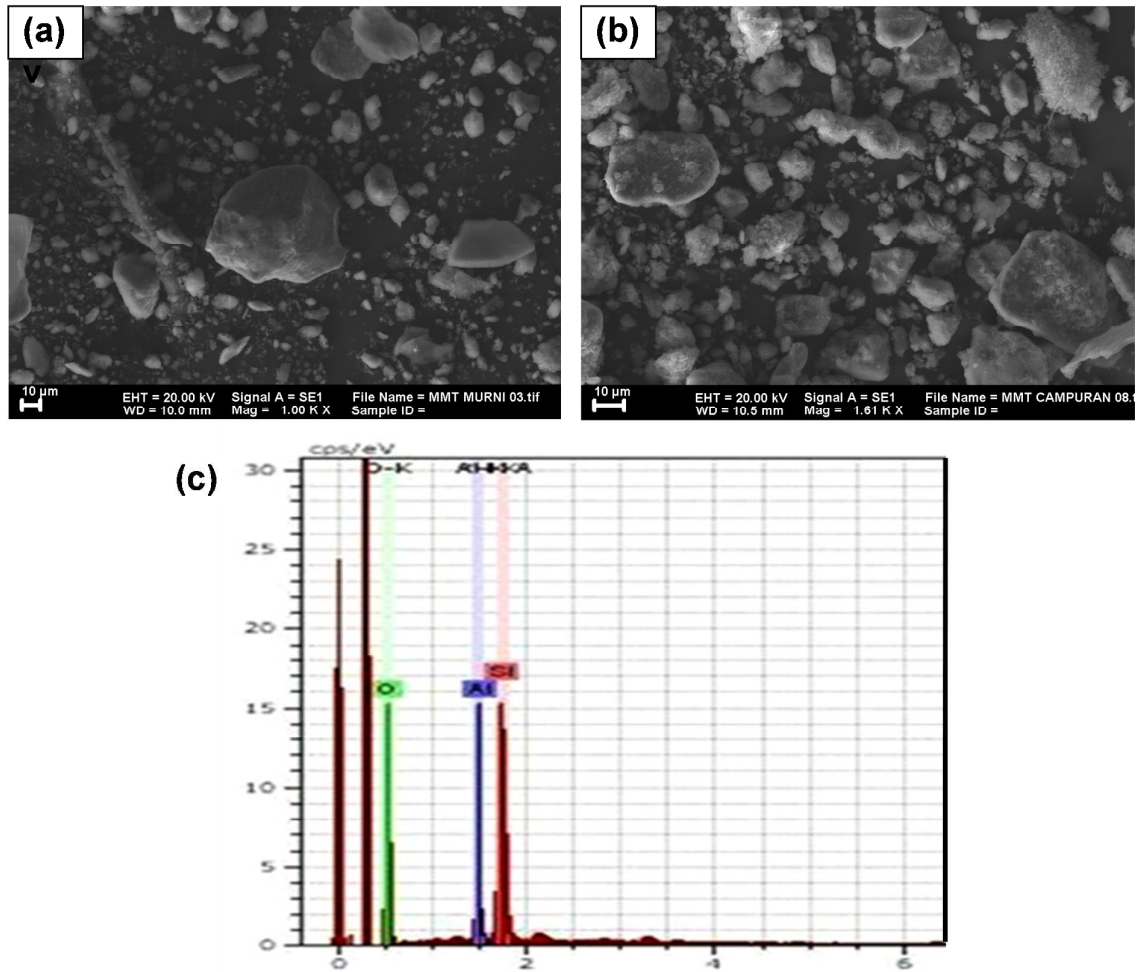


Fig.1 SEM images of (a) MMT, (b) G-MMT and (c) its EDX spectra.

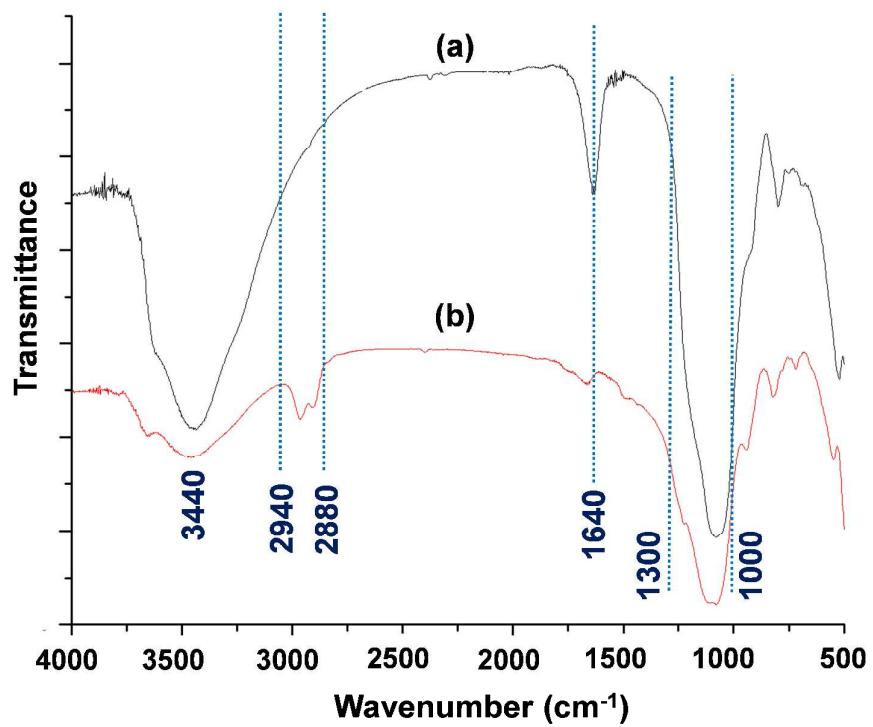


Fig. 2. FTIR spectra of (a) MMT and (b) G-MMT.

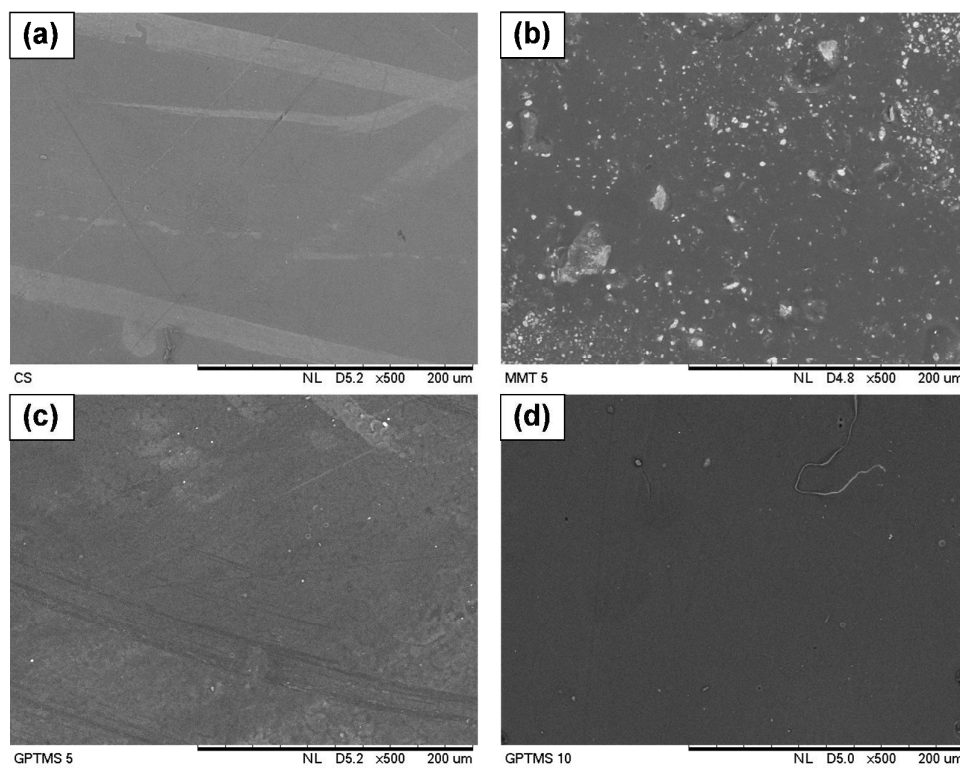


Fig. 4: SEM images of (a) pure chitosan, (b) Ch/MMT-5, (c) Ch/G-MMT-5 and (d) Ch/G-MMT-10.

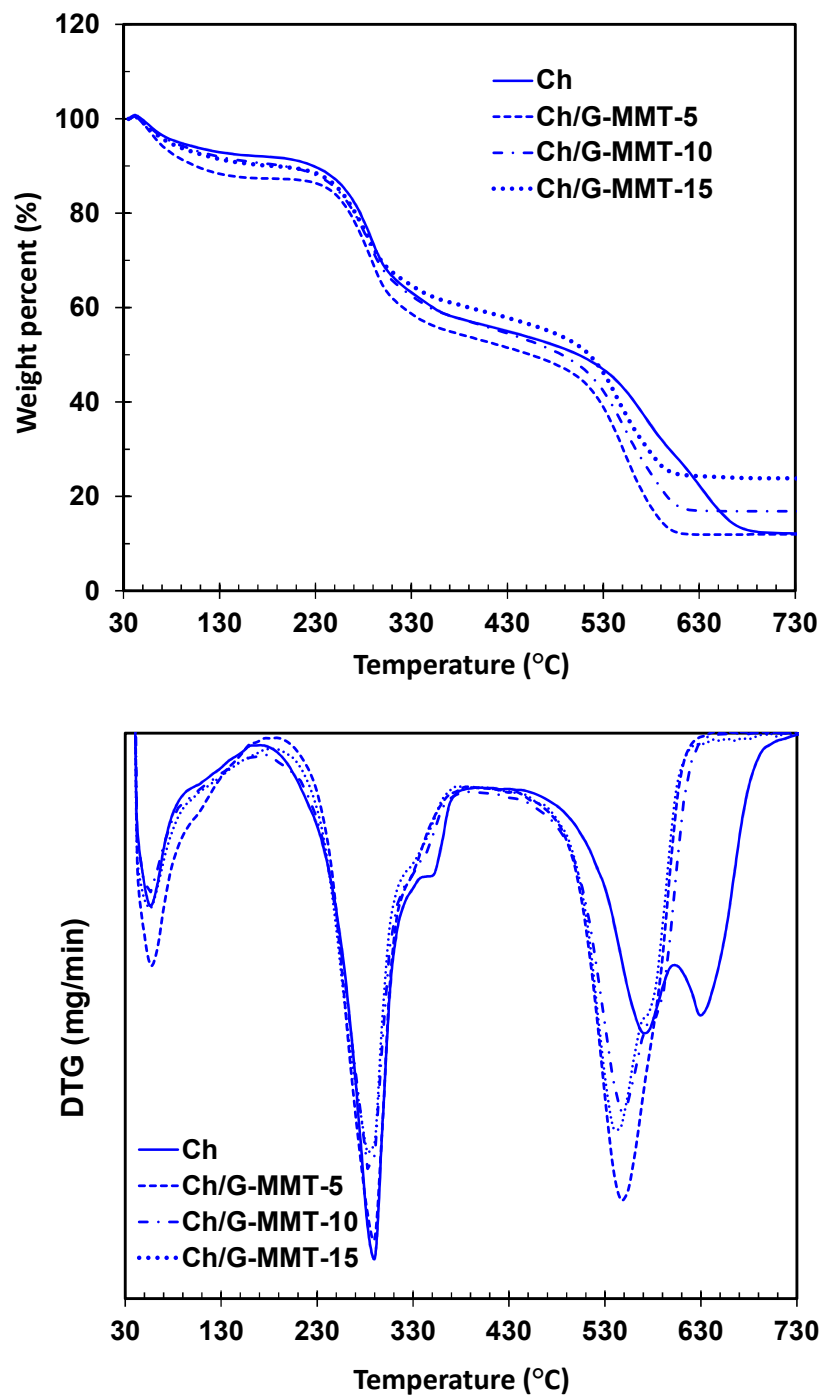


Fig. 5 TGA and DTG curves of pure chitosan (Ch) and Ch/G-MMT membrane with different G-MMT loading.

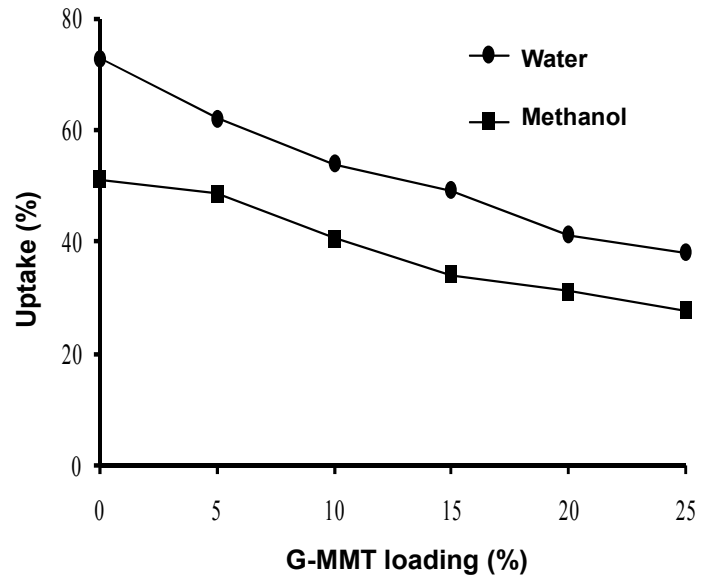


Fig. 6 Water and methanol uptake of Ch/G-MMT membranes.

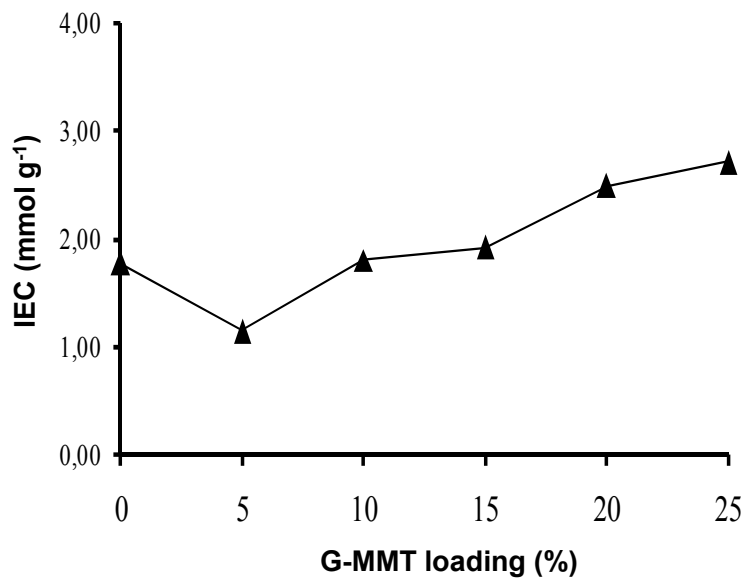


Fig. 7 IEC values of Ch/G-MMT membranes with different G-MMT loading (%).

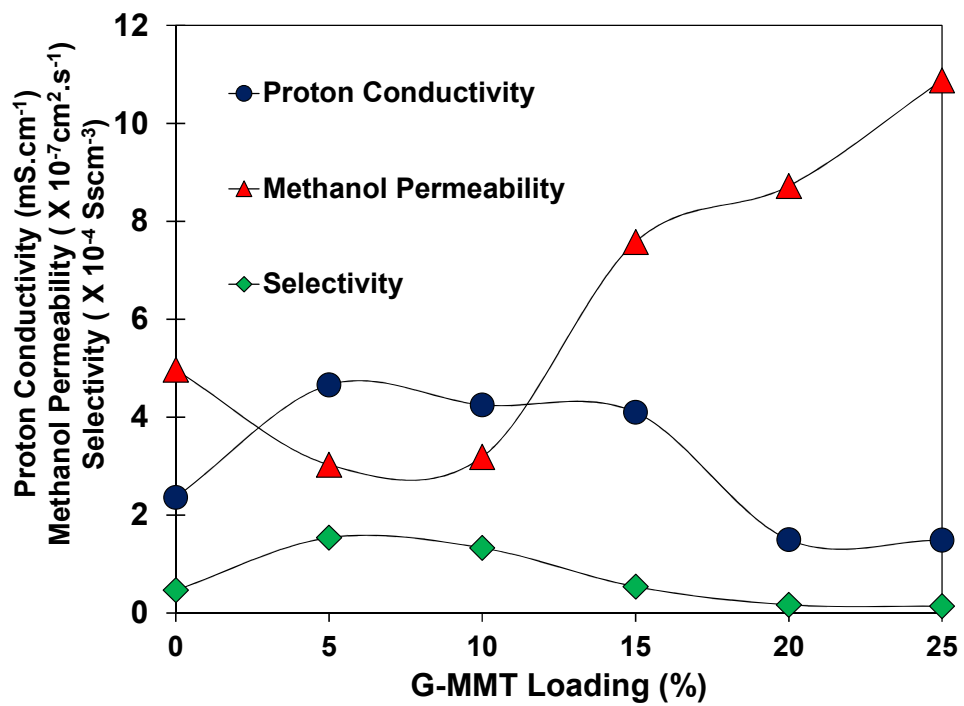


Fig. 8 Methanol permeability, proton conductivity, and relative selectivity of pure chitosan and Ch/G-MMT composite membranes with different G-MMT loading (%).

List of Table

Table 1. Compositions of Ch/G-MMT composite membranes

Membrane	Chitosan weight (g)	O-MMT weight (g)
Ch/G-MMT-5	0.95	0.05
Ch/G-MMT-10	0.90	0.10
Ch/G-MMT-15	0.85	0.15
Ch/G-MMT-20	0.80	0.20
Ch/G-MMT-25	0.75	0.25

Table 2. Methanol permeability, proton conductivity, and relative selectivity of pure chitosan and Ch/G-MMT composite membranes.

Membrane	Proton Conductivity ^a (mS.cm ⁻¹)	Methanol Permeability ^b (×10 ⁻⁷ cm ² .s ⁻¹)	Selectivity (×10 ⁴ Sscm ⁻³)	Reference
Chitosan*	2.36	4.97	0.47	
Ch/G-MMT-5	4.66	3.03	1.54	
Ch/G-MMT-10	4.25	3.19	1.33	
Ch/G-MMT-15	4.10	7.58	0.54	
Ch/G-MMT-20	1.50	8.72	0.17	
Ch/G-MMT-25	1.49	10.88	0.14	
Nafion [®] 117	31.60	25.00	1.26	[20]
Pure Chitosan	3.40	10.00	0.34	[33]

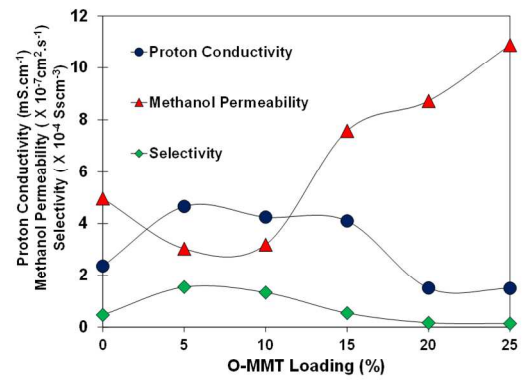
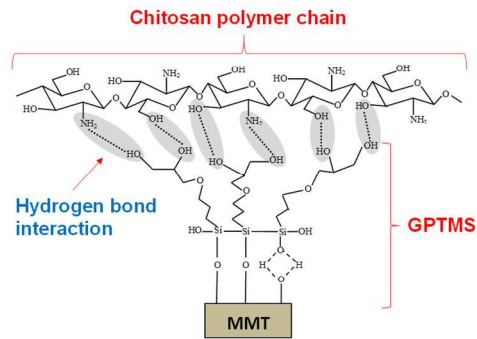
^atwo probe method, analysis using Autolab instrument

^bcell diffusion method, analysis by HPLC

*the chitosan that has been synthesis in this study

Table 3. Thermal Stability data of Ch and Ch/G-MMT 5, 10, and 15%

Sample	T _{10%} (°C)	T _{30%} (°C)	T _{50%} (°C)	DTG peak, T _{max} (°C)			Residue at 730 °C (%)
				T _{max} ¹	T _{max} ²	T _{max} ³	
Ch	220.9	298.4	500.9	56.4	290.6	575.7	12.1
Ch/G-MMT 5	107.3	290.3	459.8	56.4	290.3	546.8	13.0
Ch/G-MMT 10	197.8	298.0	490.7	56.4	290.3	546.4	16.9
Ch/G-MMT 15	190.1	298.1	514.5	56.4	286.4	554.8	23.8



263x111mm (150 x 150 DPI)